Impact of salinity gradient, water pollution and land use types on greenhouse gas emissions from an urbanized estuary

Long Ho[1]*, Matti Barthel[2], Diego Panique-Casso[1], Kaat Vermeulen[1], Stijn Bruneel[1], Xingzhen Liu[1], Samuel Bodé[3], Johan Six[2], Pascal Boeckx[3], Peter Goethals[1]

[1] *Department of Animal Sciences and Aquatic Ecology, Ghent University, Gent, Belgium;*

[2] *Department of Environmental Systems Science, ETH Zurich, Zurich, Switzerland;*

[3] *Department of Green Chemistry and Technology, Isotope Bioscience Laboratory - ISOFYS, Ghent University, Ghent, Belgium;*

* Corresponding author. Email: Long.TuanHo@UGent.be

Abstract

Estuaries have been recognized as one of the major sources of greenhouse gases (GHGs) in aquatic systems; yet we still lack insights into the impact of both anthropogenic and natural factors on the dynamics of GHG emissions. Here, we assessed the spatiotemporal dynamics and underlying drivers of the GHG emissions from the Scheldt Estuary with a focus on the effects of salinity gradient, water pollution, and land use types, together with their interaction. Overall, we found a negative impact of salinity on carbon dioxide (CO_2) and nitrous oxide (N_2O) emissions which can be due to the decrease of both salinity and water quality when moving upstream. Stronger impact of water pollution on the GHG emissions was found at the freshwater sites upstream compared to saline sites downstream. In particular, when water quality of the sites reduced from good, mainly located in the mouth and surrounded by arable sites, to polluted, mainly located in the upstream and surrounded by urban sites, CO_2 emissions from the sites doubled while N_2O emissions tripled. Similarly, the effects of water pollution on methane (CH_4) emissions became much stronger in the freshwater sites compared to the saline sites. These decreasing effects from upstream to the mouth were associated with the increase in urbanization as sites surrounded by urban areas released on average almost two times more CO_2 and N_2O than sites surrounded by nature and industry areas. Applied machine learning methods also revealed that, in addition to salinity effects, nutrient and organic enrichment stimulated the GHG emissions from the Scheldt Estuary. These findings highlight the importance of the interaction between salinity, water pollution, and land use in order to understand their influences on GHG emissions from dynamic estuarine systems.

Keywords: greenhouse gas; water pollution; estuary; Scheldt Estuary; salinity; land use;

1. Introduction

Supporting essential biogeochemical processes that are central to the Earth's functioning, estuaries play an important role in carbon (C) and nitrogen (N) cycling (Frankignoulle et al., 1998; Park et al., 2023). Apart from serving as sinks for C and N elements, they also act as a natural source of greenhouse gases (GHGs) to the atmosphere. In particular, estuaries have long been recognized as one of the major sources

of nitrous oxide (N_2O) in marine systems, which has become increasingly intensified because of eutrophication and water pollution (Ma et al., 2019). Similarly, estuaries are often supersaturated in carbon dioxide (CO_2) and methane (CH_4) because of riverine and terrestrial inputs, diffusion from sediments, surface runoff, and groundwater, and microbial processes (Belliard et al., 2022; Cotovicz et al., 2021; Yoon et al., 2017). Furthermore, since estuaries are often characterized by broad biogeochemical gradients and complex dynamics of river–sea transition zones, their GHG emissions have been reported with large spatiotemporal variability (Musenze et al., 2014).

The spatiotemporal variability of estuarine conditions and GHG emissions has often been associated to salinity gradient (Wang et al., 2017a). In particular, because the major C inputs of estuarine waters are derived from upstream rivers, concentrations of organic carbon (OC), together with CO_2 and CH_4 production, generally show a decrease from fresh to saline waters (Abril and Borges, 2005). Furthermore, from source to mouth of a river**,** the elevated salinity can inhibit growth of microorganisms and alter microbial pathways of organic matter decomposition, which thus hinders the GHG production in estuary systems (Wang et al., 2017a). Due to this complexity and multitude of potentially affecting factors, the reported emissions of estuarine ecosystems in regard to salinity gradient have been variable. Neubauer (2013) revealed that elevated salinity caused a decrease of 55% in ecosystem productivity and 30% in CH_4 production in a tidal freshwater marsh. On the other hand, Weston et al. (2011) indicated an elevation in microbial C mineralization because of salt-water intrusion, which led to a significant increase in CH_4 fluxes regardless of the increased rates of sulfate reduction. Contradicting with the redox gradient theory where methanogenesis is typical outcompeted by sulphate reduction in high salinity systems, our findings suggest a complex relationship between salinity and CH_4 emissions which can depend on specific environmental conditions and microbial community. Similar complexity has been found for CO_2 emissions: while Marton et al. (2012) found no effect of elevated salinity on CO_2 emissions, Brouns et al. (2014) indicated a reduction of 40-60% in CO_2 production due to salinization. Similarly, little consensus was found for a salinity tipping point at which the production of GHGs is significantly affected (Wang et al., 2017b). For example, Poffenbarger et al. (2011) showed no significant changes in CH_4 emissions when salinity increased from fresh (< 0.5 ppt) to mesohaline (5-

18 ppt) marshes while Chambers et al. (2011) described a near-complete reduction of CH_4 production (up to 94% less than freshwater) when salinity increased from 4.5 to 14 ppt.

Recent findings revealed that water pollution and anthropogenic changes in surrounding land use and land cover (LULC) could considerably amplify riverine GHG emissions as elevated emissions have been reported in sites that are in the vicinity of draining farmlands and urban areas (Cotovicz et al., 2021; David et al., 2018; Galantini et al., 2021). After entering the flowing waterbodies, sewage discharges and agricultural runoff, which contain high amounts of C- and N-based compounds, increase nutrient levels and worsen water quality, eventually causing an increase in GHG emissions from rivers and estuaries (Nguyen et al., 2022; Park et al., 2023). It was found that polluted rivers in urban areas produced four times more CO_2 and N_2O than pristine rivers surrounded by nature areas while this ratio was 25 times in case of CH_4 (Ho et al., 2022). Given the rapid progress of global urbanization, the role of urbanized rivers and estuaries has become crucial in global GHG emissions (Belliard et al., 2022; Gao et al., 2022; Zheng et al., 2022).

Rapid changes in land use have put immense pressures on estuarine systems, which has caused dramatic shifts in water quality, changes in streamflow and salinity, and subsequent effects on estuarine habitats (Freeman et al., 2019). While monitoring systems have been well established in response to these pressures, research on their effects on GHG emissions from estuaries remains limited. Specifically, the estuarine GHG dynamics and their driving factors remain poorly understood and quantified (Gao et al., 2022; Nguyen et al., 2022). A handful of studies have shown that pollution can be a main driver of estuarine GHG emissions (Ho et al., 2022; Ho et al., 2021a; Nguyen et al., 2022; Park et al., 2023; Yoon et al., 2017); however, to our knowledge, no studies have investigated the interactive effects of the anthropogenic pollution effects and natural salinity gradients on estuarine GHG dynamics. Building upon these perspectives, this study aims to address the following research hypothesis in the context of estuarine emissions: salinity, water pollution, land use types, and their interactions will have an impact on GHG emissions from urbanized estuaries. To do so, we conducted a case study in the Scheldt Estuary. Being home to more than 10 million inhabitants, the Scheldt Estuary has long been experiencing intensive human interventions, including vessel transportation, sediment dredging and removal,

agricultural run-off, and discharges from urban sewage systems (Comer-Warner et al., 2018). These anthropogenic activities have been contaminating water quality and modifying river flow, which can turn the Scheldt to become a 'hotspot' of GHGs emissions. Specifically, we conducted four campaigns within two years in the Scheldt Estuary, measuring fluxes and concentrations of the three main GHGs, CO_2, CH_4, and N_2O, along with physiochemical, hydromorphological, and meteorological variables. At each sampling site, we calculated the Prati water quality index and categorized types of adjacent landscapes to investigate their impact on the variation of GHG emissions. Thereby, this study was able to deliver novel insights into the GHG emissions from estuaries and their driving factors, which are essential to developing mitigation strategies in similar environmental settings.

2. Materials and Methods

2.1. Data collection

2.1.1. Study area

Samples were taken along the Scheldt Estuary that stretches from Ghent (Belgium) to Vlissingen (the Netherlands), the mouth of the Scheldt in the North Sea (Figure 1). The estuary is divided into two parts: 1) the Sea Scheldt: from the Dutch/Belgian border until Ghent and 2) the Western Scheldt from the Dutch/Belgian border to the mouth (Schepers et al., 2018).The total length of the study area is 156 km while the area of the Scheldt basin is approximately 21,863 km² which is mainly surrounded by urban and industrial areas (Schepers et al., 2018). The average population density of the basin is 477 inhabitants per km², corresponding to more than 10 million people residing in this area (Meire et al., 2005). In summer, the average air temperature is 17.9 °C and the average precipitation 234.2 mm while in winter this is respectively 4.1 °C and 228.6 mm. The salinity of the Scheldt Estuary fluctuates from 0.2 to 30.1 PSU (Meire et al., 2005).

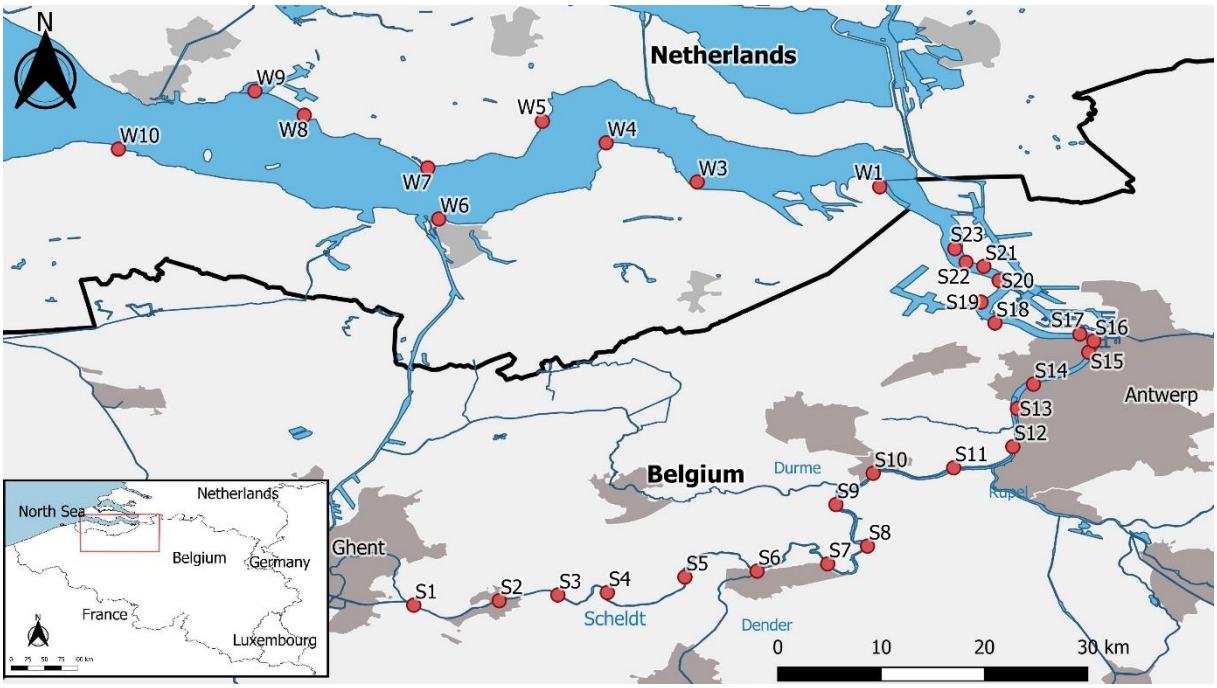

Figure 1. Location of the study area and the 32 sampling sites of the four sampling campaigns, two in winter and two in summer. The red dots represent the sites that were sampled during all campaigns. S is short for Sea Scheldt and W for Western Scheldt. Urban areas are indicated in grey. Note that W10 is located at the mouth of the Scheldt Estuary.

2.1.2. Field measurements

Four sampling campaigns were conducted, one in the winter of 2021 (from 08/02/2021 to 12/03/2021), one in the summer of 2021 (from 16/08/2021 to 15/09/2021), one in the winter 2022 (from 31/01/2022 to 11/02/2022) and one in the summer of 2022 (from 01/08/2022 to 11/08/2022). During all sampling campaigns 32 sampling sites were visited: 23 sites in the Sea Scheldt and 9 sites in the Western Scheldt (Figure 1). Besides measuring fluxes and dissolved concentrations of CO_2, CH_4, and N_2O, we also collected physicochemical and meteorological data. In particular, dissolved oxygen (DO), water temperature, pH, total dissolved solid (TDS), and turbidity were determined by a handheld multiprobe (YSI 9620v2-2 version 1.2, YSI Xylem Inc., Yellow Springs, Ohio, USA). Calibration was performed prior to sampling and supplemented with an inspection after sampling. Each measurement was repeated three times at every site to ensure the stability of the multiprobe and water conditions.

Water samples from all sampling sites were transported in a cooler and then preserved in a refrigerator until analysis. We used Merck kits to measure nutrient contents of the samples, including ammonium (NH_4^+), nitrate (NO_3^-), nitrite (NO_2^-), orthophosphate (PO_4^{3-}), total nitrogen (TN), and total phosphorus (TP) spectrophotometrically (low-range Merck test kits with AquaMate, Thermo Spectronic, S1). More

detailed information about the Merck kits can be found in **Table S9.1**. The analysis of organic carbon (OC) content, including total carbon (TC) and total organic carbon (TOC), was done by the Laboratory of Analytical Chemistry and Applied Ecochemistry (Ecochem) at Ghent University using a TOC/TN analyzer (Shimadzu TOC V CPN-analyzer). We followed the standards of APHA (2022) and US EPA (2012) for quality assurance and control of the analytical measurements. Note that to examine the effects of water quality on the GHG emissions of the Scheldt Estuary, we calculated the Prati water quality index (WQI) based on various water quality parameters, such as O_2 level, OC and nutrients. Details of the calculation can be found in Ho et al. (2022).

We surveyed hydro-morphological variables of the sites and their surroundings, including land use, macrophytes, riparian vegetation, channel types, and sediment accumulation, using a modified field protocol of Ho et al. (2022). Regarding land use, we categorized them into five types in the field protocol: urban, transportation, industry, arable, and nature by evaluating the land use surrounding each site within a stretch of 100 m x 10 m on both river banks. In addition, we collected information about river width and depth, tides, ecotopes and meteorological variables from the VNSC at https://www.scheldemonitor.be, and from Flemish and Dutch monitoring stations at https://waterinfo.be and https://www.rijkswaterstaat.nl. We chose the stations closest to the sampling sites, their distances ranged between 3 m and 5.48 km. Note that we developed an interactive application using the **R Shiny** package (Chang et al., 2015) so users can access, analyze, and visualize the collected data that are available online at https://env-research.shinyapps.io/Scheldt_GHGs/.

2.1.3. GHG fluxes

To measure the fluxes of CO_2, CH_4, and N_2O, we applied the floating chamber (FC) method given its simplicity and feasibility, following the guidelines of the International Hydropower Association (IHA, 2010). The deployed FCs were a circular container with a diameter of 23 cm, a height of 23 cm, a volume of 9.1 L and an area of 0.04 m^2, which was made of 3 mm thick PVC plastic and wrapped by aluminum foil to prevent heat exchange during the measurement. We wrapped a foam ring around the FCs to keep the penetration of the FCs of around six cm from the top. Furthermore, we connected an anchor to the center of the FCs with a string to keep them stable on the water surface. We used a polyurethane tube

158 that was connected near to the top of the FCs to vent the pressure inside the FCs when placing the FCs
159 on the water surface and then we submerged the tube after the water level reached the foam ring. We
160 collected gas samples from the headspace of the FCs via a butyl rubber stopper that was embedded on
161 top of the FCs and then stored into evacuated 12 mL Exetainer vials (Exetainer®, Labco Ltd, High
162 Wycombe, UK). We collected three samples at 0, 20, and 40 minutes after placement in order to
163 determine the fluxes of CO_2, CH_4, and N_2O. By using gas chromatography, the sampled vials were then
164 analyzed at ISOFYS, Ghent University (Shimadzu GC-14B, equipped with a double 1/8'OD, 0.085'ID,
165 1 + 2m, Porapak Q 80/100, and an ECD detector) and ETH Zurich (Bruker, GC-456, Scion Instruments,
166 Livingston, UK). Gas fluxes were calculated based on the following equation:

167 Flux = Slope × Volume of chamber × (Area of chamber)$^{-1}$ (Eq. 1)

168 The slope was calculated based on the linear regression of gas concentration in the FCs versus time.
169 Details of the R^2 values can be found in **Figure S10.1**.

170 *2.1.4. Dissolved gas concentrations*

171 Prior to sample collection, 12 mL vials with airtight septa (Exetainer®, Labco Ltd, High Wycombe,
172 UK) were pre-conditioned with 50µL of 50% $ZnCl_2$ as a preservative agent before capping and flushing
173 with high purity N_2 (Alphagaz 2, Carbagas, Gümlingen, Switzerland). At each sampling, we collected
174 6 mL of water into the vials resulting in a final headspace pressure of around 2 atm. Note that we
175 carefully removed air bubbles from the water samples prior to injection into the vial. We measured the
176 concentrations of CO_2, CH_4, and N_2O in the headspace using gas chromatography at ISOFYS, Ghent
177 University and ETH Zurich. We calibrated the instrument during the measurement of each gas using
178 several sets of standards. Dissolved gas concentrations (µMol L^{-1}) were calculated using Henry's law
179 considering the volume of the vials and headspace.

180 $$C_{aq} = p_a \times k_h \quad \text{(Eq. 2)}$$

181 where k_h is Henry's constant adjusted for lab temperature (mol m^{-3} Pa^{-1}) and p_a is the partial pressure
182 of the gas in the headspace (Pa^{-1}). We corrected the effects of salinity on gas solubility using Sechenov
183 equation (Hermann et al., 1995).

2.2. Data analysis

2.2.1. Mixed models

To investigate the impact of salinity, water pollution, land use types, and their interactions on the GHG fluxes from the Scheldt, we applied mixed models in R (R Core Team, 2014) using the **lme4** package (Bates et al., 2015). Specifically, while the GHG fluxes were considered as response variables and analyzed separately, we took into account all of the collected variables as predictors, and seasons (winter and summer) and rivers (Sea Scheldt and Western Scheldt) as random variables in the mixed models. Prior to the modelling, the GHG fluxes were natural log-transformed and all continuous predictors were standardized (values minus the mean and divided by the standard deviation) to improve the performance of the model and increase the interpretability of the results (Zuur and Ieno, 2016). To avoid model overfitting (Ho and Goethals, 2022), we selected the most parsimonious model by comparing the AICs of all models with a condition of keeping salinity and either water quality or land use in the model since they are critical in driving estuarine GHG emissions. We used the 'dredge' function in the **muMIn** package to generate the most parsimonious model (Barton and Barton, 2014). Among the equivalent models ($\Delta AIC \leq 2$), we chose the model with the highest weight value (Chen et al., 2022). We used the variance inflation factors (VIFs) to examine the multicollinearity among predictors in the most parsimonious models and found that all predictors had VIF < 3, indicating no multicollinearity in the most parsimonious models (Zuur et al., 2010). Finally, we displayed the interactions between salinity, water quality and land-use types with interaction plots using the **interactions** package v.1.1.5 (Long, 2019). Specifically, the **interactions** package provides a convenient framework for modeling and analyzing interactions between variables in mixed models via creating interaction terms, visualization and interpretation.

2.2.2. Combination of PCA and K-means clustering

We applied a combination of Principal component analysis (PCA) and K-means clustering to determine how much of the variance of the data can be explained by the measured variables in order to unravel the nature of the underlying processes of estuarine GHG production (Tabachnick and Fidell, 2012). Prior to

the PCA, we standardized the data to avoid the biases of PCA by the scale of the variables (Manly and Alberto, 2016). In the K-means clustering, we applied the Elbow method to determine the optimal number of clusters. In particular, we tested the algorithm with the number of clusters up to 10 and in every test and calculated the Within Cluster Sum of Squares (WCSS) which measures the squared average distance of all the points within a cluster to the cluster centroid (Han et al., 2012). The optimal number of clusters was chosen when the decrease in WCSS becomes marginal, meaning that the increase in the number of clusters gives no significant improvement in the clustering. In this study, the data was partitioned based on GHG emissions. After determining the optimal number of clusters, the clusters were presented in the biplots depicting the PCs that explained most of the variance. Combining the two aforementioned methods allowed to identify and quantify the patterns of the underlying processes affecting the emissions of each cluster. PCA and K-means clustering were respectively implemented via **stats** (R Core Team and Worldwide Contributors, 2002) and **clusterR** (Mouselimis et al., 2019) packages in R.

2.2.3. Random forests

To identify the main factors driving the spatiotemporal variation in GHG emissions, random forests (RFs) were implemented in R (R Core Team, 2014) via the **ranger** package (Wright and Ziegler, 2017). We applied the same model inputs, including all of the collected variables, and outputs, including the three GHG fluxes, as in the mixed models for training the random forests. To optimize the models, we tuned two essentials hyperparameters, including the minimal size of a node (*min.node.size*) and the number of candidate variables considered at each split (*mtry*) while the number of trees (*num.trees*) as a not tunable parameter was set sufficiently high, i.e. 500 (Probst et al., 2019). To do so, the **mlr** package of Bischl et al. (2016) was applied in parallel on eight CPU cores. The tuned model with optimal hyperparameters was run to identify the importance of variables for the GHG fluxes. Permutation accuracy importance was preferred over the conventional variable importance since it can deal with the drawbacks of the latter, such as bias towards continuous variables compared to categorical variables and sensitivity with missing data and outliers (Strobl et al., 2007).

3. Results and discussion

3.1. Spatiotemporal variability of estuary GHG dynamics

To investigate the dynamics of biogeochemical processes and GHG production in the Scheldt Estuary, we measured various physicochemical variables and GHG emissions in the Scheldt which differed notably between the two parts of the Scheldt (**Figures 2, S1.1 and S1.2**). Specifically, the average emissions of CO_2 and N_2O from the Sea Scheldt were around five times higher than those from the Western Scheldt, i.e., 3.9 ± 0.2 g CO_2 m^{-2} d^{-1} and 1.2 ± 0.1 mg N_2O m^{-2} d^{-1} from the Sea Scheldt compared to 0.7 ± 0.1 g CO_2 m^{-2} d^{-1} and 0.30 ± 0.04 mg N_2O m^{-2} d^{-1} from the Western Scheldt. On the other hand, CH_4 emissions were relatively the same between both parts, on average 7.5 ± 1.2 mg CH_4 m^{-2} d^{-1} in the Sea Scheldt and 9.6 ± 2.3 mg CH_4 m^{-2} d^{-1} in the Western Scheldt. Compared to global estimates of riverine GHG fluxes, i.e. 9,900 g CO_2 m^{-2} yr^{-1} (Liu et al., 2022), 41.4 g CH_4 m^{-2} yr^{-1} (Stanley et al., 2022), and 0.22 g N_2O m^{-2} yr^{-1} (Maavara et al., 2019), the Scheldt Estuary emitted less than around 10 times of CO_2 and CH_4 fluxes while its N_2O emissions were about 1.5 times higher. Nutrients and OC concentrations increased when moving upstream: up to two times more of TOC, three times more of TN, and two times more of TP were found in the Sea Scheldt than in the Western Scheldt. This can be attributed to two factors: nutrient dilution by the North Sea and higher urbanization in upper part of the Scheldt Estuary. Previous studies also found a decrease in concentrations of nutrients and OC when moving seawards because of dilution effects from the North Sea (Fang et al., 2019; Fleming-Lehtinen et al., 2015; Gross et al., 2022; Martens, 2019). Higher nutrient concentrations found in the freshwater discharge from the Sea Scheldt were associated with higher urbanization in this area: the further upstream, the more urbanized areas (**Figure S4.1**).

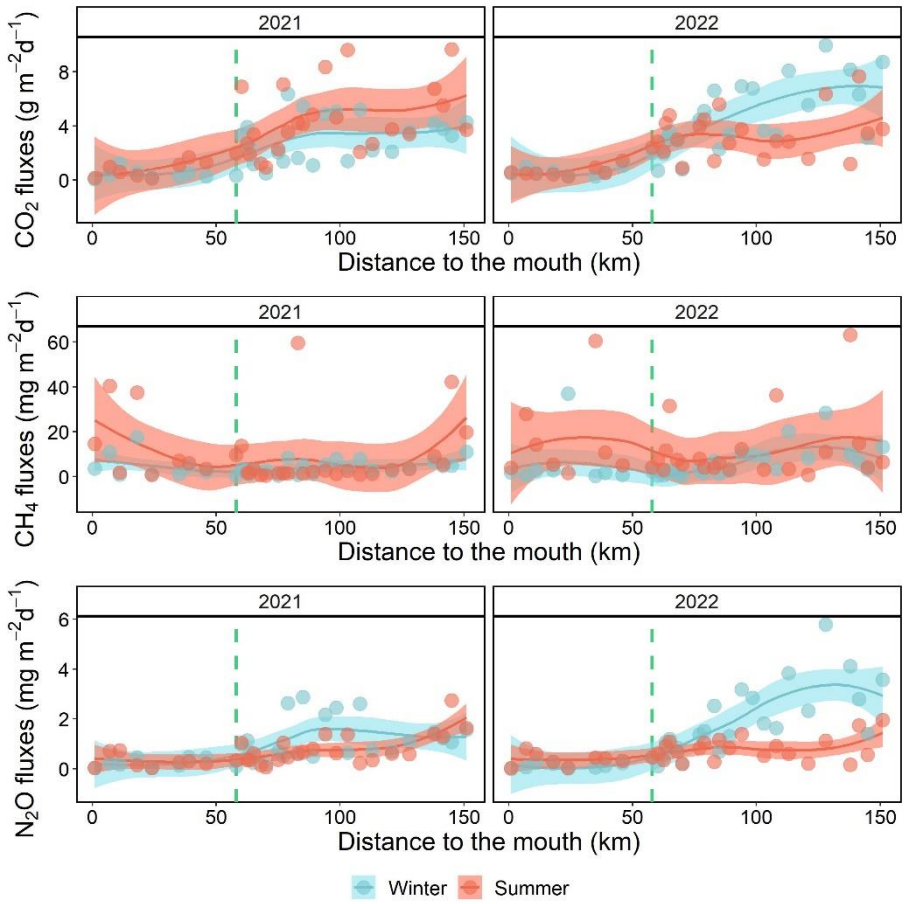

Figure 2. GHG emissions from the Scheldt Estuary. The trend lines represent the central tendency of variable patterns in two seasons as characterized by a loess curve with 95% confidence intervals shaded between the upper and lower bands. The vertical line represents the border between Sea Scheldt and Western Scheldt. Exact *p* values of the Wilcoxon Rank Sum test for comparison between two seasons and between two rivers can be found in **Tables S1.1 and S1.2**.

Regarding the temporal variation, we found that the GHG emissions remained relatively stable between the two years, while CH_4 and N_2O emissions showed a moderate difference between summer and winter (**Tables S1.2 and S1.3**). In particular, the Scheldt emitted double the amount of CH_4 in summer compared to winter, i.e., 10.9 ± 1.9 and 5.3 ± 0.8 mg m^{-2} d^{-1}, respectively, while the levels of the N_2O emissions increased from around 0.68 ± 0.07 mg m^{-2} d^{-1} in summer to 1.21 ± 0.16 mg m^{-2} d^{-1} in winter. On the other hand, the emissions of CO_2 kept stable around 3.0 ± 0.2 mg m^{-2} d^{-1}. Note that while the seasonal variation of the CH_4 emissions occurred in both Sea Scheldt and Western Scheldt, the N_2O emissions only varied across the two seasons in the Sea Scheldt and remained stable seasonally in the Western Scheldt. Furthermore, we found higher DO level of 10.9 ± 0.05 mg O_2 L^{-1} in winter compared to its summer values of 6.9 ± 0.1 mg O_2 L^{-1}. Similarly, the concentration of N species was higher in winter than summer: 20 times higher for NH_4^+ and two times higher for NO_2^- and NO_3^-, which can be

attributed to much lower N leaching from agricultural activities during summers (Billen et al., 2005).. Moreover, we observed two opposite trends of TOC and TIC levels between the two seasons: while TIC concentrations decreased by around 1.5 times, TOC concentrations doubled from summer to winter. These fluctuations in the C and N species imply that higher microbial activity, including nitrification, denitrification, C mineralization, took place in summer which caused lower concentrations of O_2, OC and N species because of their consumption (Ho et al., 2021b). Furthermore, although warmer summers can enhance algal activities leading to lower inorganic carbon (IC), higher TIC in summer in our case suggests that discharges of OC were the major driver of the IC pool, which is in agreement with previous studies (Amann et al., 2015; Atkins, 2017).

3.2. Effects of salinity

To assess the effects of salinity on the GHG dynamics of the Scheldt, we categorized the estuary into four classes: fresh (< 0.5 PSU), oligohaline (0.5-5 PSU), mesohaline (5-18 PSU) and polyhaline waters (18-30 PSU) according to the Venice salinity system (Figure 3). We found significant differences of CO_2 and N_2O emissions across the salinity classes while the CH_4 emissions on average remained relatively unchanged despite the substantial variation of their values in each salinity class. In particular, the emissions of CO_2 decreased gradually when the sites became more saline: 4.8 ± 0.4 g CO_2 m^{-2} d^{-1} in freshwater, 2.9 ± 0.3 g CO_2 m^{-2} d^{-1} in oligohaline, 2.3 ± 0.3 g CO_2 m^{-2} d^{-1} in mesohaline, and 0.6 ± 0.1 g CO_2 m^{-2} d^{-1} in polyhaline waters. Similarly, when the salinity increased by one level, the N_2O emissions decreased by about half: 1.70 ± 0.18 mg N_2O m^{-2} d^{-1} in freshwater, 0.73 ± 0.08 mg N_2O m^{-2} d^{-1} in oligohaline, 0.48 ± 0.07 mg N_2O m^{-2} d^{-1} in mesohaline, and 0.28 ± 0.05 mg N_2O m^{-2} d^{-1} in polyhaline waters. These decreases led to the declining trend of global warming potential (GWP) values with the increase of the salinity level regardless of the wide variation of the CH_4 emissions across the salinity classes. This implies that freshwater rivers could contribute more to warming climate than their counterparts located near the coastal areas.

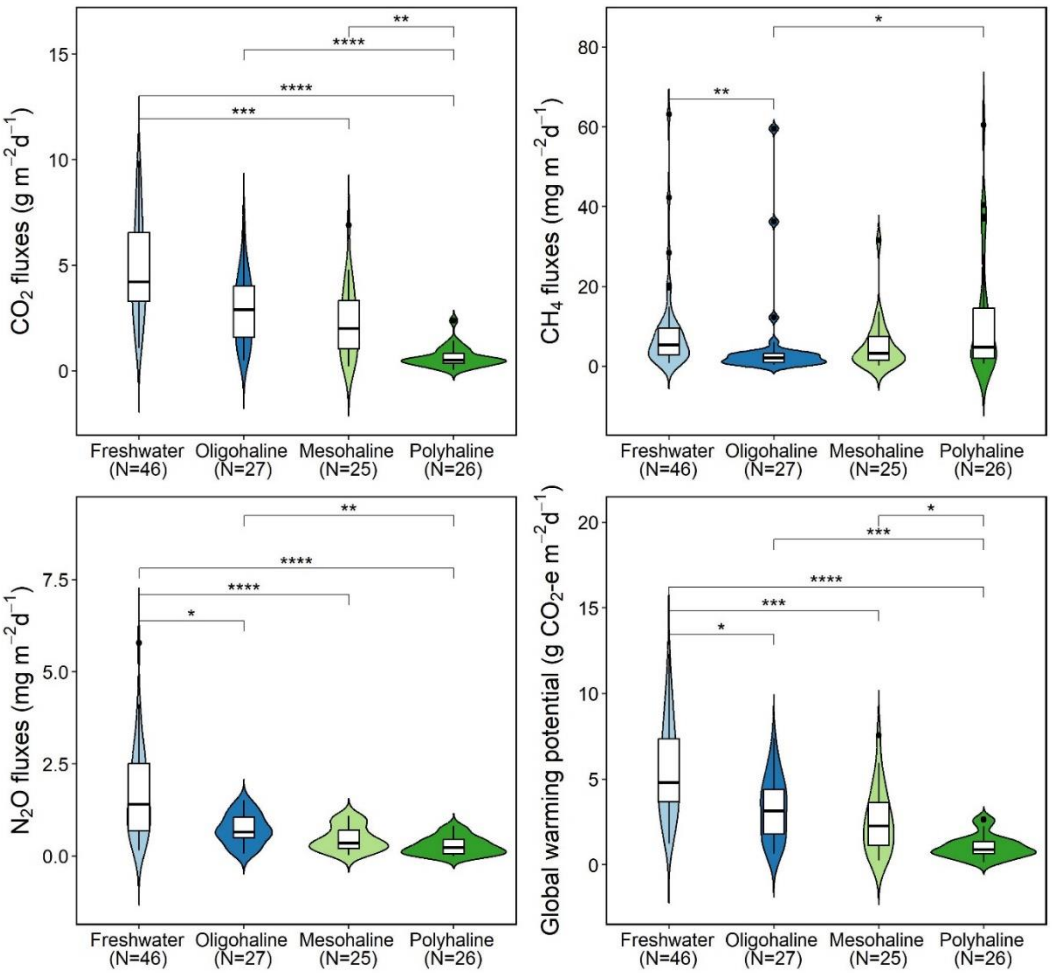

297

298 **Figure 3**. GHG fluxes and their global warming potential from the Scheldt Estuary in different salinity categories using the
299 Venice system: freshwater (<0.5 PSU), oligohaline (0.5-5 PSU), mesohaline (5-18 PSU) and polyhaline water (18-30 PSU).
300 The violin plots include box plots showing median, lower (Q1) and upper (Q3) quartiles and 1.5 times the length of the
301 interquartile range of GHG fluxes. Note that the violin plots also depict distribution of the data of which the width
302 corresponds to the frequency of data points in the distribution. Kruskal–Wallis tests followed by Bonferroni–Dunn test were
303 applied for multiple comparisons between different salinity categories. $^{*}p \leq 0.05$, $^{**}p \leq 0.01$, $^{***}p \leq 0.001$, $^{****}p \leq 0.0001$.
304 Exact *p* values of the Kruskal Wallis with Bonferroni-Dunn for multiple comparison between salinity categories can be found
305 in **Table S1.4.**

306 Although saline waters can considerably alter microbial pathways of OC and nutrient decomposition via
307 inhibitory impact of osmotic stress and high concentrations of saline-induced toxic products, reports on
308 the effects of elevated salinity riverine emissions have been inconsistent (Wang et al., 2017a). For
309 example, methanogens are likely to be outcompeted by sulfate-reducing bacteria that can steer
310 biogeochemical processes towards the production of CO_2 rather than CH_4 as indicated in Neubauer
311 (2013); they found that elevated salinity caused a decrease of 30% in CH_4 production in a tidal
312 freshwater marsh. In contrast, Wilson et al. (2015) found no significant differences in CH_4 emissions
313 across different salinity levels in the Gulf of Mexico Estuary, which was also the case of the Scheldt
314 Estuary. The wide variation of CH_4 emissions with several extremely high fluxes in all the salinity levels

suggests the contribution of ebullition in the Scheldt which is inherently a sporadic process that could be missed by short deployment of our FCs. The ebullition fluxes can be notably disturbed in case of the Scheldt where large scale dredging remains a common practice to guarantee safe access to the port of Antwerp (Martens, 2019). Regarding the CO_2 and N_2O emissions, their negative correlation with salinity (**Figure S2.1**) could be confounded by the increase of pH and the decrease of NO_3^-, TN and TOC when moving downstream. Specifically, lower pH at the upstream sites led to higher availability of H^+ which could react with HCO_3^-, causing the shift of the equilibrium towards the reaction of HCO_3^- and hence more CO_2 production. Higher NO_3^-, together with more availability of OC and less inhibitory effects of lower saline waters, also facilitated the production of N_2O (Wang et al., 2017a). Brouns et al. (2014) found similar findings in their experiment that indicates a reduction of 40-60% in CO_2 production with the elevated salinity.

3.3. Effects of water pollution

According to the Prati water quality index, we found that majority of the sites in the Scheldt acquired either good or acceptable water quality while only three sites were categorized as heavily polluted (**Figure 4**). Note that while good water quality sites were located mainly in polyhaline and mesohaline waters, (heavy) polluted water quality sites were located mainly in fresh and oligohaline waters which were surrounded mainly by urban and industrial areas (**Figure S3.1**). This implies the impact of discharges from these built-up areas on the enrichment of OC and nutrients in the Scheldt, which in turn affected the GHG emissions from the sites. We observed an increase in CO_2 and N_2O emissions when the water quality of the sites exacerbated from good to acceptable and to polluted. Specifically, when water quality of the sites reduced from good to polluted, CO_2 emissions from the sites doubled while their N_2O emissions tripled. Contrary to the expectation that polluted sites would release more CH_4 as observed in previous studies (Nguyen et al., 2022; Park et al., 2023), there was insignificant difference of CH_4 emissions across the water quality categories despite their large variation in each water quality category.

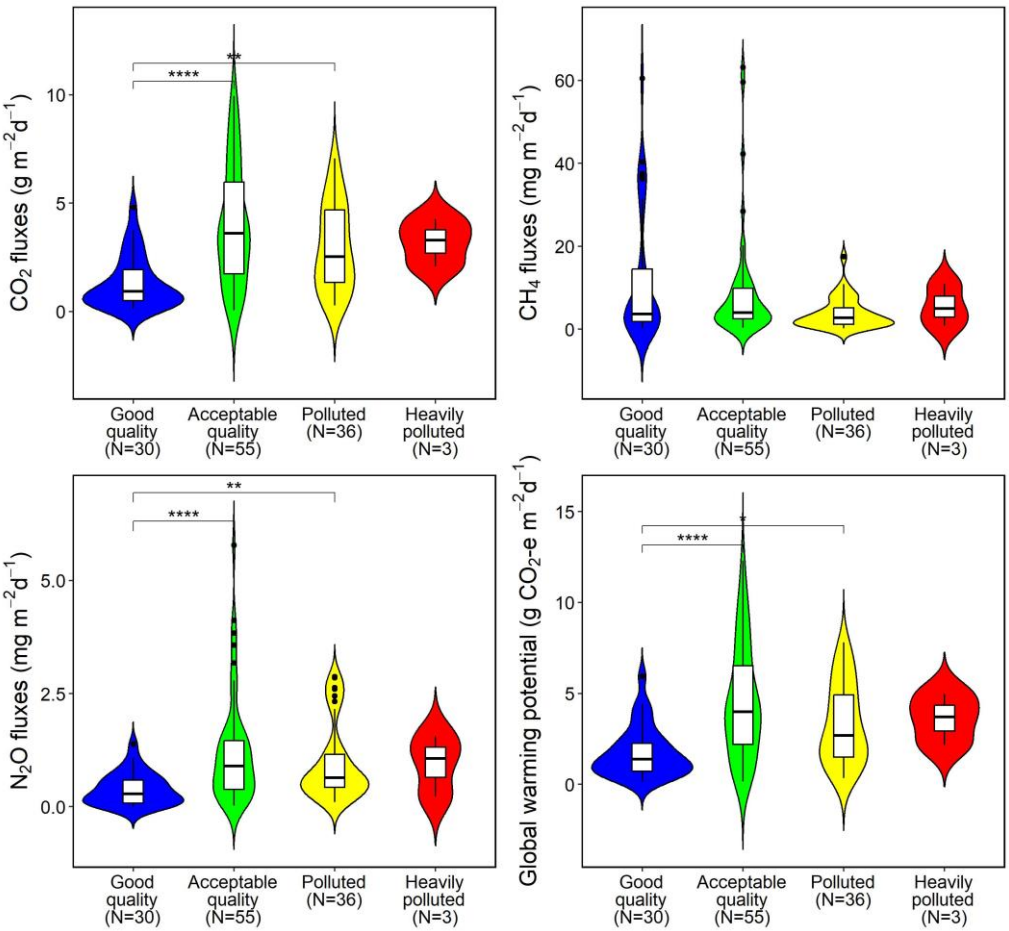

340

341 **Figure 4**. GHG fluxes from the Scheldt Estuary in different water quality categories using Prati Water Quality Index. The
342 violin plots include box plots showing median, lower (Q1) and upper (Q3) quartiles and 1.5 times the length of the
343 interquartile range of GHG fluxes. Note that the violin plots also depict distribution of the data of which the width
344 corresponds to the frequency of data points in the distribution. Kruskal–Wallis tests followed by Bonferroni–Dunn test were
345 applied for multiple comparisons between different water quality categories. $^{*}p \leq 0.05$, $^{**}p \leq 0.01$, $^{***}p \leq 0.001$, $^{****}p \leq$
346 0.0001. Exact *p* values of the Kruskal Wallis with Bonferroni-Dunn for multiple comparison between salinity categories can
347 be found in **Table S1.5**.

348 To investigate the potential interactive effects of salinity and water quality on GHG emissions from the
349 Scheldt, we used their interaction term in the mixed models (**Table S3.1**) and then visualized it in the
350 interactive plots (**Figure 5**). Specifically, the relatively parallel lines delineating the evenly decreasing
351 CO_2 emissions with salinity in four water quality categories indicate the strong negative effects of
352 salinity on CO_2 emissions regardless of the water quality of the sites while the effects of water quality
353 on the CO_2 emissions remained relatively unchanged along the salinity gradient. On the other hand,
354 because of stronger interaction, the effects of water quality on CH_4 emissions was much more
355 pronounced when sites were less saline or, in other words, when moving upstream. Furthermore, when
356 sites were polluted, salinity had negative impacts on CH_4 emissions while an increase in salinity had
357 relatively no impact on CH_4 emissions when the water quality of the sites was acceptable or good. The

intersecting lines in case of N_2O implies strong interactive effects between both variables: the N_2O emissions from (heavily) polluted sites changed in the opposite direction compared to those from good/acceptable quality sites when moving from freshwater to saline sites. Besides, we found larger differences across the water quality categories at the freshwater than saline sites, indicating stronger impact of water quality on GHG emissions upstream compared to at the mouth of the Scheldt. This finding is in line with studies in other estuaries where pollution in upper parts of the estuaries was the main source of estuarine GHG emissions (Nguyen et al., 2022; Park et al., 2023; Yoon et al., 2017).

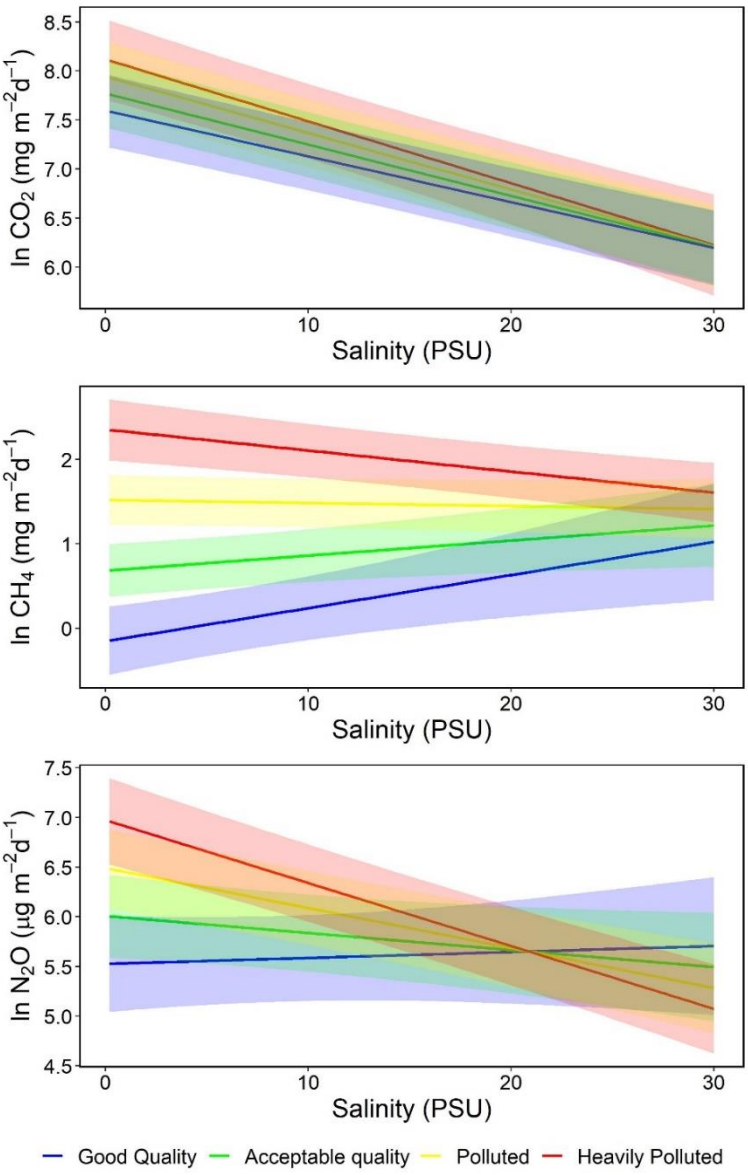

Figure 5. Interactive effects of salinity and water pollution on the greenhouse gas emissions from the Scheldt Estuary. The lines represent the predicted value of the greenhouse gas emissions across four water quality categories with 95% confidence intervals shaded between the upper and lower bands.

3.4. Effects of land use types

The results from the field protocol indicated that most of urban sites are located upstream while most of the industrial sites are located near the port of Antwerp (**Figure S4.1**). It is important to note that half of these built-up sites were classified as (heavily) polluted according to Prati Index (**Figure S4.2**). Furthermore, we found that urban sites released the most of CO_2 and N_2O, i.e., 4.28 ± 0.38 g CO_2 m^{-2} d^{-1} and 1.35 ± 0.14 mg N_2O m^{-2} d^{-1}, followed by sites surrounded mainly by nature, industry and transportation while sites surrounded mainly by agriculture areas emitted the least (**Figure 6**). Comparing across the land-use types, urban sites released on average almost two times more CO_2 and N_2O than nature and industry sites, and six times more than agriculture sites. No significant difference of CH_4 emissions were found across the land-use types (exact *p* values can be found in **Table S1.6**). Consequently, sites surrounded by urban areas had the highest GWP of 4.86 ± 0.42 g CO_2-e m^{-2} d^{-1}, followed by nature sites with 3.50 ± 0.54 g CO_2-e m^{-2} d^{-1}, industry sites with 2.85 ± 0.35 g CO_2-e m^{-2} d^{-1}, transportation sites with 1.79 ± 0.63 g CO_2-e m^{-2} d^{-1}, and agriculture sites with 1.07 ± 0.17 g CO_2-e m^{-2} d^{-1}. Also noteworthy is that we found high and widely fluctuating emissions of all three GHGs from sites surrounded mainly by nature in the Scheldt Estuary, which is in disagreement with previous studies (Brown et al., 2022; Ho et al., 2022; Nguyen et al., 2022) that found natural sites to release the less GHGs compared to more anthropogenic sites. This contradiction can be attributed to a highly fragmented nature and landscape of Flanders (De Keersmaeker et al., 2015), which hence diminishes the impact of these areas on improving river water quality and thereby reducing GHG emissions.

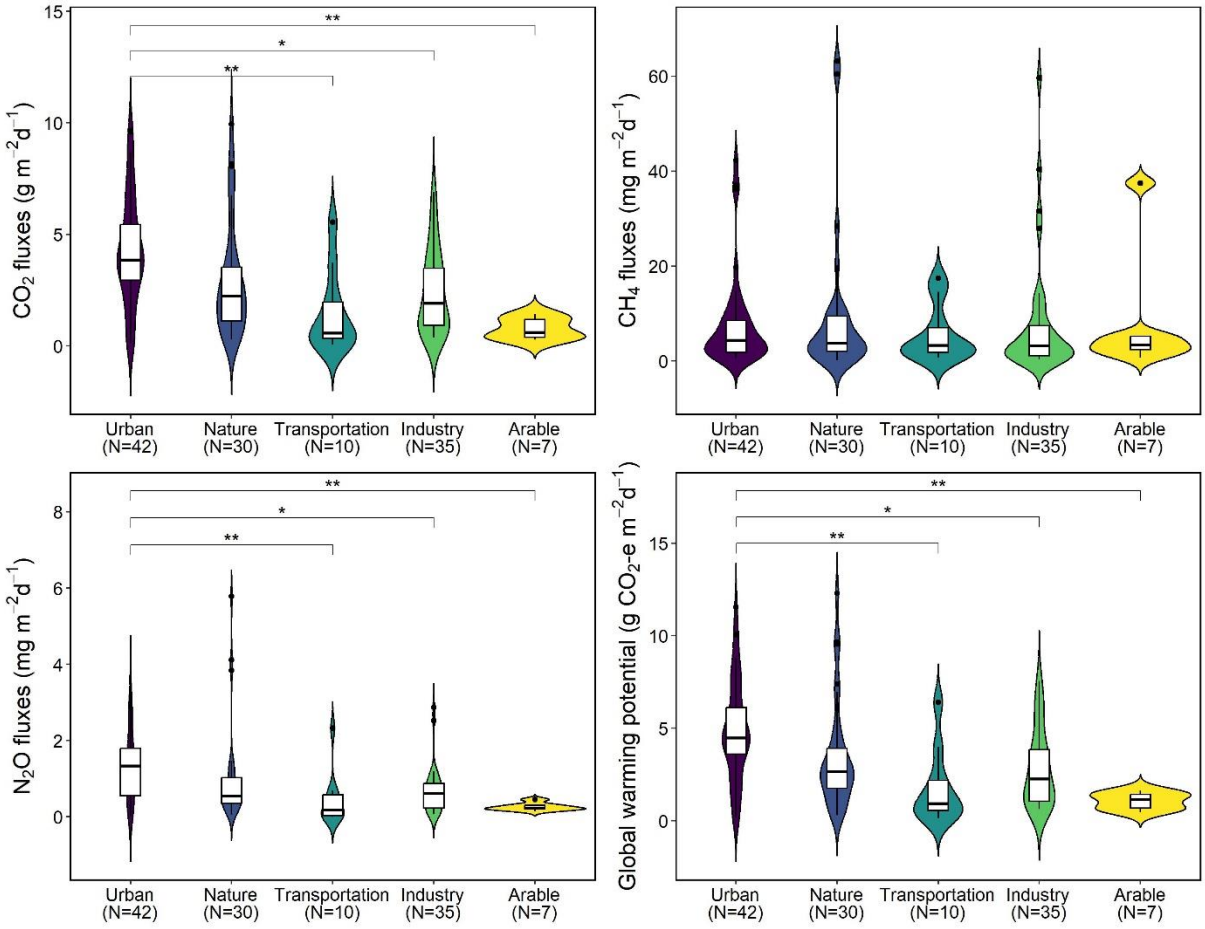

388

389 **Figure 6**. GHG emissions of the Scheldt Estuary in different land-use types. The violin plots include box plots showing
390 median, lower (Q1) and upper (Q3) quartiles and 1.5 times the length of the interquartile range of GHG fluxes. Note that the
391 violin plots also depict distribution of the data of which the width corresponds to the frequency of data points in the
392 distribution. Kruskal–Wallis tests followed by Bonferroni–Dunn test were applied for multiple comparisons between
393 different land-use types. $^{*}p \leq 0.05$, $^{**}p \leq 0.01$, $^{***}p \leq 0.001$, $^{****}p \leq 0.0001$. Exact p values of the Kruskal Wallis with
394 Bonferroni-Dunn for multiple comparison between salinity categories can be found in **Table S1.6**.

395 To investigate the potential interactive effects of salinity and land use types on GHG emissions from the
396 Scheldt, we used their interaction term in the mixed models (**Table S4.1**) and then visualized it in the
397 interactive plots (**Figure 7**). The intersecting lines suggest strong interactive effects between the two
398 variables on the emissions of all GHGs: the emissions from urban sites changed in the opposite direction
399 compared to those from arable sites when moving from freshwater to saline sites. Specifically, higher
400 emissions can be found at the urban sites in the upstream part compared to the other sites; however, this
401 gap disappeared gradually and went in the opposite direction when the sites became saline. In fact, from
402 upstream to mouth, while the emissions from urban sites decreased substantially, the emissions from
403 arable sites had an upward tendency, especially in case of the CH_4 emissions. Furthermore, when
404 investigating the interactive effects of salinity and water pollution in each land use type, we found only

marginal effects on GHG emissions from sites surrounded by urban and nature areas, which is in contrast to the strong interactions found at sites surrounded by arable, transport or industrial areas (**Figures S5.1, S5.2, and S5.3**). This implies that there were strong positive impacts of urban land use on GHG emissions from the Scheldt, which is in contrast to the negative impacts of natural sites regardless of the water quality conditions and salinity levels at the sites. On the other hand, at the sites surrounded by the other land use types, GHG emissions strongly depended on the interactive effects of salinity and water pollution. Recently, the strong positive impacts of urbanization on estuarine GHG emissions have also been reported in other studies as a result (un)treated wastewater discharges (Nguyen et al., 2022; Park et al., 2023; Yoon et al., 2017). To our knowledge, this is the first study that indicates the crucial roles of the interactive effects between salinity, water pollution and land use types on estuarine GHG emissions. Its specific conclusions should be extrapolated to other estuaries with caution since each estuary has its own characteristics regarding water quality and surrounding landscape. For this reason, it can be beneficial to have more data collected from various estuaries with different water quality conditions and surrounding land use types. Furthermore, the cumulative effects of land use types on water quality and consequently elevated GHG emissions from rivers and estuaries should be further investigated.

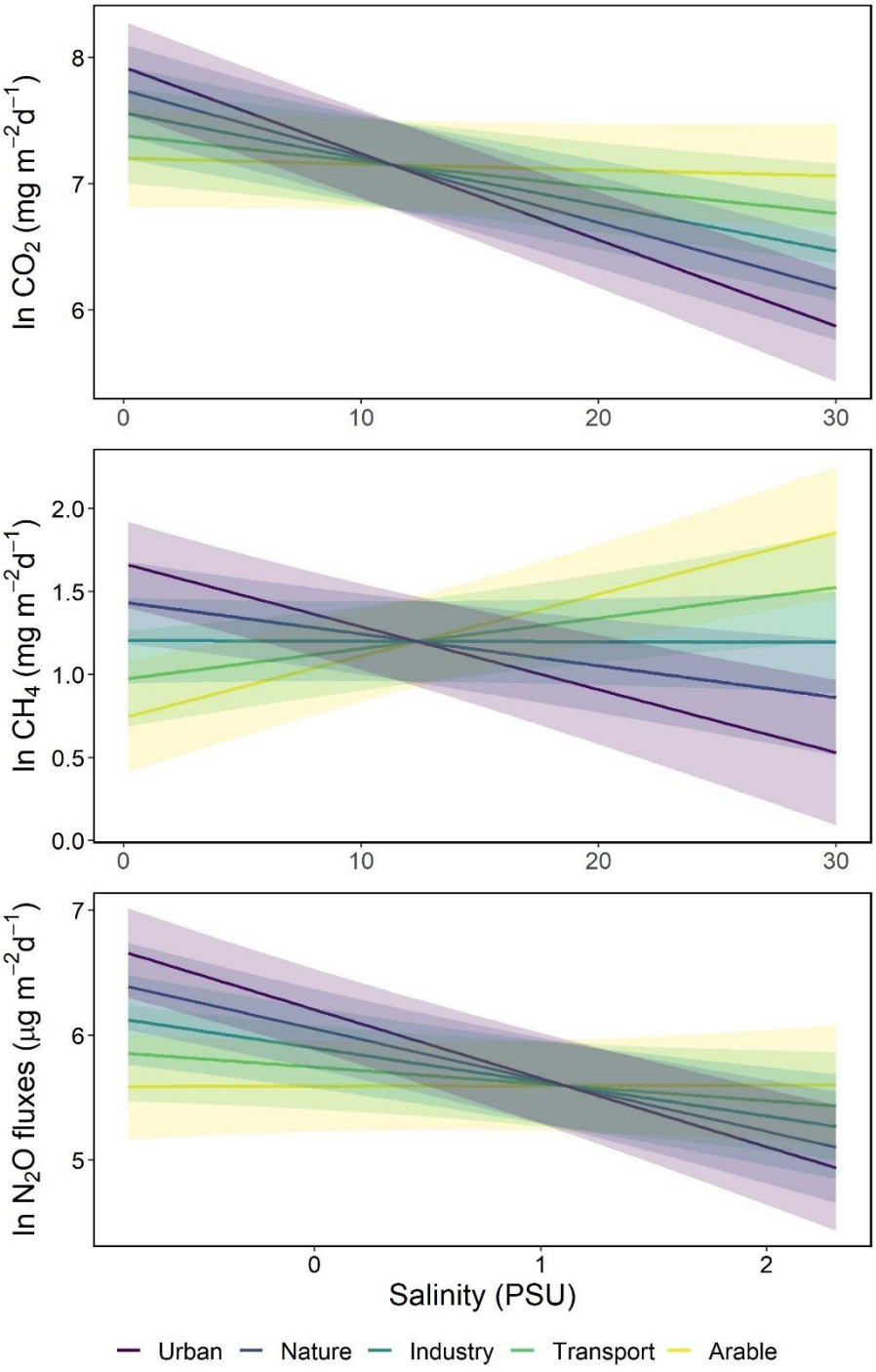

Figure 7. The interactive effects of the salinity and land use types on the greenhouse gas emissions from the Scheldt Estuary. The lines represent the predicted value of the greenhouse gas emissions across the five land use categories with 95% confidence intervals shaded between the upper and lower bands.

3.5. Influencing factors on estuary GHG dynamics

PCA was combined with the K-means clustering to reveal how environmental variables affected the GHG emissions. Firstly, we found that five clusters were optimal based on the Elbow Method (**Figure S7.1**), which are represented in different colors in the biplots of PCA in Figure 8. The description of the

clusters in regard to the GHG emissions can be found in S7 in the SM. Indicating the weights of the variables to reconstruct each PC, the loading coefficients in **Table S7.1** shows that air temperature (0.38), DO (-0.34), and NO_3^- (-0.30) had the highest correlation coefficients with PC1 while TC (0.39), salinity (0.34), and TIC (0.31), were the most correlated component loadings of PC2. These coefficients indicate the positive or negative correlations between these variables and the PCs, from which we can conclude how these variables affected the data of different clusters. From this analysis, it can be noted that the availability of IC concentrations affected positively the CO_2 emissions which is also the case of the impact of N species on N_2O emissions. Furthermore, the higher the salinity level of a site was, the smaller were its CO_2 and N_2O emissions. Similarly, it appears that higher pH affected negatively the N_2O emissions from the Western Scheldt possibly by retarding microbial activity, including nitrification and denitrification processes (Goncalves et al., 2015). The presence of extreme values of CH_4 emissions in different clusters confirm the sporadic nature of the ebullitive emissions, which requires appropriate monitoring methods for assessments, such as bubble traps and hydroacoustic surveys (DelSontro et al., 2015).

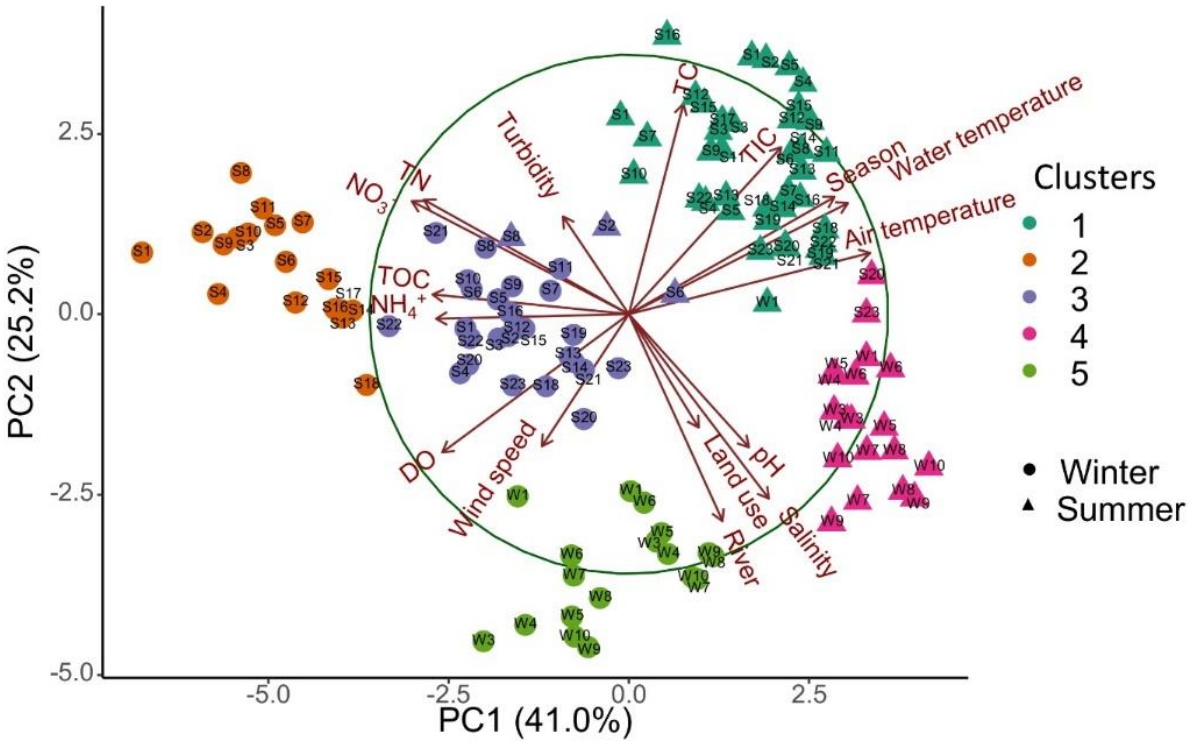

Figure 8. Biplots of the first two principal components (PCs) which is labeled according to the five K-means clusters (colors) and season (shapes).

To identify the main important factors explaining the GHG emissions, we applied random forest based variable importance analysis that indicated the effects of the factors in changing the GHG emissions from the sites (Figure 9). Overall, salinity was among the top important variables affecting the variations of the three gases. However, it is important to bear in mind the strong association between the increase of salinity and the reduction of organic matter and nutrients because of the dilution effect: the closer to the mouth, the lower became the levels of C and N species. This association confounds the impact of salinity on the emissions from the Scheldt Estuary with the impact of the other variables. In particular, chemical equilibria of the IC species appear to be the dominant process affecting the CO_2 fluxes as pH, TIC and TC are among the top important variables. We observed that the closer to the mouth, the higher was the pH and the lower were the CO_2 fluxes, indicating that when moving downstream of the Scheldt, the lower availability of H^+ to react with HCO_3^- caused the shifts of the equilibrium towards the production of more HCO_3^- and hence less CO_2. To further investigate the role of organic carbon in the production of CO_2, it is recommended to analyze dissolved and particulate organic carbon for better representation of the carbon source in estuarine systems. Similarly, the elevation of N_2O fluxes can be attributed to the decrease in salinity level and the increase in NO_3^- concentrations when moving upstream of the estuary where more urbanization and higher NO_3^- from wastewater discharges were found. While higher NO_3^- concentrations enabled more N_2O production, lower salinity level in the Sea Scheldt alleviated the inhibition of osmotic stress and saline-induced toxic products, including H_2S, HS^-, S^{2-}, and Cl^- (Wang et al., 2017a). Although CH_4 emissions from the Scheldt appear sporadic as shown in previous figures, the importance analysis revealed that temperature, DO, organic matter and salinity affected CH_4 production the most. While the first three factors directly influence methanogenesis, methanogens in saline waters were likely to be outcompeted by sulfate-reducing bacteria that could utilize hydrogen and acetate at lower concentrations, hence, constrained methane production (Belliard et al., 2022). To further investigate the major CH_4 and N_2O production pathways, position isotopic analysis (Yu et al., 2020) and molecular analyses on the abundance and expression of key functional genes (Gallarotti et al., 2021) are highly recommended.

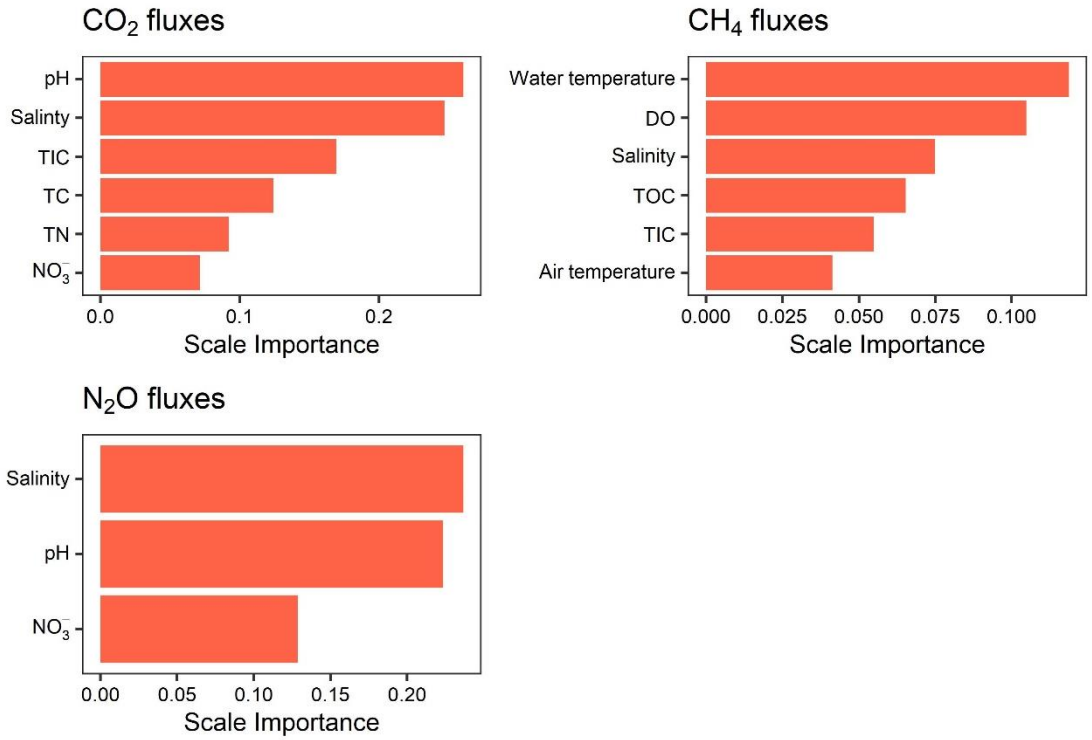

Figure 9. Permutation accuracy importance of variables in the variation of GHG fluxes from the Scheldt Estuary. The presented variables have *p*-value larger than 0.05, meaning they have significant impact on the variation of the GHG emissions.

4. Conclusion

- The interactions between salinity, water pollution and land use play a crucial role in the dynamics of biogeochemical processes and GHG production in the Scheldt Estuary. Overall, we found significant differences of CO_2 and N_2O emissions across the salinity classes while the CH_4 emissions on average remained relatively stable. However, the negative correlation of CO_2 and N_2O emissions with salinity could be affected by the increase of pH and the decrease of NO_3^-, TN and TOC when moving downstream.
- An increase in CO_2 and N_2O emissions was observed when water quality of the sites exacerbated from good to acceptable and to polluted while no significant difference of CH_4 emissions could be found across different water quality categories. Specifically, when water quality of the sites reduced from good to polluted, CO_2 emissions from the sites doubled while their N_2O emissions tripled. Regarding the interaction between salinity and water quality, higher emissions were released from (heavily) polluted sites compared to good/acceptable quality sites in the upstream

part; however, this gap shrunk gradually and went in the opposite direction when the sites became saline. Besides, we found larger fluctuation across the water quality categories at the freshwater sites compared to that at the saline sites, indicating stronger impact of water quality on the GHG emissions in the upstream compared to that in the mouth of the estuary.

- Comparing across the land-use types, urban sites released on average almost two times more CO_2 and N_2O than nature and industry sites, and six times more than agriculture sites. On the other hand, no significant difference of the CH_4 emissions across the land-use types was found. Moving downstream, while the emissions from urban sites decreased substantially, the emissions from arable sites had an upward tendency, especially in case of the CH_4 emissions. Furthermore, when investigating the interactive effects of salinity and water quality in each land use type, we found only marginal effects on the emissions from sites surrounded by urban and nature areas which is in contrast to strong interaction that was found in sites surrounded by arable, transport and industrial areas.
- This study highlights the importance of taking into account the interaction between salinity, water pollution, and land use in order to understand the influencing factors of GHG emissions from dynamic estuarine systems.

Acknowledgement

We are grateful to the VLIZ (Vlaams Instituut voor de Zee) for the use of the Zeekat and support in logistics for planning of the sampling. We thank De Vlaamse Waterweg nv and Rijkswaterstaat for allowing us to conduct the sampling campaigns in the Scheldt Estuary. We thank Nico De Maerteleire and Sébastien Pieters from Research Institute for Nature and Forest (NIBO), and Tom Moens, Pieterjan Verhelst and Carl van Colen from Faculty of Sciences at UGent for their support with the field work. Long Ho is a postdoctoral fellow supported by the Research Foundation of Flanders (FWO) (project number 1253921N).

References

Abril, G. and Borges, A.V. (2005) Greenhouse Gas Emissions — Fluxes and Processes: Hydroelectric Reservoirs and Natural Environments. Tremblay, A., et al. (eds), pp. 187-207, Springer Berlin Heidelberg, Berlin, Heidelberg.

Amann, T., et al. 2015. Inorganic Carbon Fluxes in the Inner Elbe Estuary, Germany. Estuar Coast 38(1), 192-210.

APHA 2022. Standard methods for the examination of water and wastewater. American Public Health Association (APHA): Washington, DC, USA.

Atkins, M.L.S., I. R.: Maher, D. T. 2017. Seasonal exports and drivers of dissolved inorganic and organic carbon, carbon dioxide, methane and δ13C signatures in a subtropical river network. Sci Total Environ 575, 545-563.

Barton, K. and Barton, M.K. 2014. Package 'MuMIn'. Version 1, 18.

Bates, D., et al. 2015. Fitting Linear Mixed-Effects Models Using lme4. J Stat Softw 67(1), 1-48.

Belliard, J.-P., et al. 2022. Carbon dynamics and CO2 and CH4 exchange in the mangrove dominated Guayas river delta, Ecuador. Estuarine, Coastal and Shelf Science 267, 107766.

Billen, G., et al. 2005. Nutrient fluxes and water quality in the drainage network of the Scheldt basin over the last 50 years. Hydrobiologia 540, 47-67.

Bischl, B., et al. 2016. mlr: Machine Learning in R. The Journal of Machine Learning Research 17(1), 5938-5942.

Brouns, K., et al. 2014. The effects of salinization on aerobic and anaerobic decomposition and mineralization in peat meadows: The roles of peat type and land use. J Environ Manage 143, 44-53.

Brown, A.M., et al. 2022. Anthropogenic-estuarine interactions cause disproportionate greenhouse gas production: A review of the evidence base. Mar Pollut Bull 174.

Chambers, L.G., et al. 2011. Short-Term Response of Carbon Cycling to Salinity Pulses in a Freshwater Wetland. Soil Sci Soc Am J 75(5), 2000-2007.

Chang, W., et al. 2015. Package 'shiny'. http://citeseerx.ist.psu.edu/viewdoc/download.

Chen, X.L., et al. 2022. Meta-analysis shows that plant mixtures increase soil phosphorus availability and plant productivity in diverse ecosystems. Nature Ecology & Evolution 6(8), 1112-+.

Comer-Warner, S.A., et al. 2018. Thermal sensitivity of CO2 and CH4 emissions varies with streambed sediment properties Nat Commun 10.

Cotovicz, L.C., et al. 2021. Greenhouse gas emissions (CO2 and CH4) and inorganic carbon behavior in an urban highly polluted tropical coastal lagoon (SE, Brazil). Environ Sci Pollut R 28(28), 38173-38192.

David, F., et al. 2018. Carbon biogeochemistry and CO2 emissions in a human impacted and mangrove dominated tropical estuary (Can Gio, Vietnam). Biogeochemistry 138(3), 261-275.

De Keersmaeker, L., et al. 2015. The analysis of spatio-temporal forest changes (1775-2000) in Flanders (northern Belgium) indicates habitat-specific levels of fragmentation and area loss. Landscape Ecology 30(2), 247-259.

DelSontro, T., et al. 2015. Size Does Matter: Importance of Large Bubbles and Small-Scale Hot Spots for Methane Transport. Environ Sci Technol 49(3), 1268-1276.

Fang, X., et al. 2019. Spatio-temporal variation in sediment ecosystem processes and roles of key biota in the Scheldt estuary. Estuarine, Coastal and Shelf Science 222, 21-31.

Fleming-Lehtinen, V., et al. 2015. Organic Carbon Concentration in the Northern Coastal Baltic Sea between 1975 and 2011. Estuar Coast 38(2), 466-481.

Frankignoulle, M., et al. 1998. Carbon dioxide emission from European estuaries. Science 282(5388), 434-436.

Freeman, L.A., et al. 2019. Impacts of Urbanization and Development on Estuarine Ecosystems and Water Quality. Estuar Coast 42(7), 1821-1838.

Galantini, L., et al. 2021. How Are Greenhouse Gases Coupled Across Seasons in a Large Temperate River with Differential Land Use? Ecosystems.

Gallarotti, N., et al. 2021. In-depth analysis of N2O fluxes in tropical forest soils of the Congo Basin combining isotope and functional gene analysis. The ISME Journal.

Gao, D.Z., et al. 2022. N2O emission dynamics along an intertidal elevation gradient in a subtropical estuary: Importance of N2O consumption. Environ Res 205.

Goncalves, C., et al. 2015. Tidal and spatial variability of nitrous oxide (N2O) in Sado estuary (Portugal). Estuar Coast Shelf S 167, 466-474.

Gross, E., et al. 2022. River discharge-related nutrient effects on North Sea coastal and offshore phytoplankton communities. J Plankton Res 44(6), 959-972.

Han, J., et al. (2012) Data Mining: Concepts and Techniques, Elsevier.

Hermann, C., et al. 1995. The Estimation of Gas Solubilities in Salt-Solutions. Chem Eng Sci 50(10), 1673-1675.

Ho, L. and Goethals, P. 2022. Machine learning applications in river research: Trends, opportunities and challenges. Methods Ecol Evol 13(11), 2603-2621.

Ho, L., et al. 2022. Greenhouse gas dynamics in an urbanized river system: influence of water quality and land use. Environ Sci Pollut R 29(25), 37277-37290.

Ho, L., et al. 2021a. Integrated mechanistic and data-driven modeling for risk assessment of greenhouse gas production in an urbanized river system. J Environ Manage 294, 112999.

Ho, L., et al. 2021b. Spatial and temporal variations of greenhouse gas emissions from a waste stabilization pond: Effects of sludge distribution and accumulation. Water Res 193, 116858.

IHA (2010) GHG Measurement Guidelines for Freshwater Reservoirs: Derived from: the UNESCO/IHA Greenhouse Gas Emissions from Freshwater Reservoirs Research Project, International Hydropower Association (IHA).

Liu, S.D., et al. 2022. The importance of hydrology in routing terrestrial carbon to the atmosphere via global streams and rivers. P Natl Acad Sci USA 119(11).

Long, J.A. 2019. Interactions: Comprehensive, user-friendly toolkit for probing interactions. R package version 1.1. 0. The Comprehensive R Archive Network.

Ma, L., et al. 2019. Major role of ammonia-oxidizing bacteria in N2O production in the Pearl River estuary. Biogeosciences 16(24), 4765-4781.

Maavara, T., et al. 2019. Nitrous oxide emissions from inland waters: Are IPCC estimates too high? Global Change Biol 25(2), 473-488.

Manly, B.F.J. and Alberto, J.A.N. (2016) Multivariate Statistical Methods: A Primer, Fourth Edition, CRC Press.

Martens, P.S. (2019) Characterization of the impact of dredging and disposal on the channel network of the Western Scheldt estuary, Delft University.

Marton, J.M., et al. 2012. Effects of Salinity on Denitrification and Greenhouse Gas Production from Laboratory-incubated Tidal Forest Soils. Wetlands 32(2), 347-357.

Meire, P., et al. 2005. The Scheldt estuary: A description of a changing ecosystem. Hydrobiologia 540, 1-11.

Mouselimis, L., et al. 2019. ClusterR: Gaussian Mixture Models, K-Means, Mini-Batch-Kmeans, K-Medoids and Affinity Propagation Clustering. R package version 1(0).

Musenze, R.S., et al. 2014. Methane and nitrous oxide emissions from a subtropical estuary (the Brisbane River estuary, Australia). Sci Total Environ 472, 719-729.

Neubauer, S.C. 2013. Ecosystem Responses of a Tidal Freshwater Marsh Experiencing Saltwater Intrusion and Altered Hydrology. Estuar Coast 36(3), 491-507.

Nguyen, A.T., et al. 2022. Does eutrophication enhance greenhouse gas emissions in urbanized tropical estuaries? Environ Pollut 303.

Park, J.H., et al. 2023. Basin-specific pollution and impoundment effects on greenhouse gas distributions in three rivers and estuaries. Water Res 236.

Poffenbarger, H.J., et al. 2011. Salinity Influence on Methane Emissions from Tidal Marshes. Wetlands 31(5), 831-842.

Probst, P., et al. 2019. Hyperparameters and tuning strategies for random forest. Wiley Interdisciplinary Reviews: Data Mining and Knowledge Discovery 9(3), e1301.

R Core Team 2014 R: A Language and Environment for Statistical Computing, ISBN 3-900051-07-0, Vienna, Austria.

R Core Team and Worldwide Contributors 2002. The R stats package. R Foundation for Statistical Computing, Vienna, Austria: Available from: http://www.R-project.org.

Schepers, L., et al. (2018) Landscapes and Landforms of Belgium and Luxembourg, pp. 281-296, Springer.

Stanley, E., et al. 2022 A global database of methane concentrations and atmospheric fluxes for streams and rivers ver 5375843, Environmental Data Initiative.

Strobl, C., et al. 2007. Bias in random forest variable importance measures: Illustrations, sources and a solution. Bmc Bioinformatics 8.

Tabachnick, B.G. and Fidell, L.S. (2012) Using Multivariate Statistics, Harpe rCollins College Publishers.

US EPA 2012 Selected Analytical Methods for Environmental Remediation and Recovery (SAM), U.S. Environmental Protection Agency, U.S. Environmental Protection Agency, Washington, DC.

Wang, C., et al. 2017a. Identifying the Salinity Thresholds that Impact Greenhouse Gas Production in Subtropical Tidal Freshwater Marsh Soils. Wetlands 37(3), 559-571.

Wang, X.F., et al. 2017b. Greenhouse gases concentrations and fluxes from subtropical small reservoirs in relation with watershed urbanization. Atmos Environ 154, 225-235.

Weston, N.B., et al. 2011. Accelerated microbial organic matter mineralization following salt-water intrusion into tidal freshwater marsh soils. Biogeochemistry 102(1-3), 135-151.

Wilson, B.J., et al. 2015. Spatial and temporal variability in carbon dioxide and methane exchange at three coastal marshes along a salinity gradient in a northern Gulf of Mexico estuary. Biogeochemistry 123(3), 329-347.

Wright, M.N. and Ziegler, A. 2017. ranger: A Fast Implementation of Random Forests for High Dimensional Data in C plus plus and R. J Stat Softw 77(1), 1-17.

Yoon, T.K., et al. 2017. CO2 Outgassing from an Urbanized River System Fueled by Wastewater Treatment Plant Effluents. Environ Sci Technol 51(18), 10459-10467.

643 Yu, L., et al. 2020. What can we learn from N2O isotope data? – Analytics, processes and modelling.
644 Rapid Commun Mass Sp 34(20), e8858.

645 Zheng, Y., et al. 2022. Global methane and nitrous oxide emissions from inland waters and estuaries.
646 Global Change Biol n/a(n/a).

647 Zuur, A.F. and Ieno, E.N. 2016. A protocol for conducting and presenting results of regression-type
648 analyses. Methods Ecol Evol 7(6), 636-645.

649 Zuur, A.F., et al. 2010. A protocol for data exploration to avoid common statistical problems. Methods
650 Ecol Evol 1(1), 3-14.

651